

## Cavity-ring-down spectroscopy on the oxygen A band in magnetic fields up to 20 T

Giel Berden,<sup>1</sup> Richard Engeln,<sup>1</sup> Peter C. M. Christianen,<sup>2</sup> Jan C. Maan,<sup>2</sup> and Gerard Meijer<sup>1</sup>  
<sup>1</sup>Research Institute for Materials, Department of Molecular and Laser Physics, University of Nijmegen,  
 Toernooiveld, 6525 ED Nijmegen, The Netherlands

<sup>2</sup>Research Institute for Materials, High Field Magnet Laboratory, University of Nijmegen, Toernooiveld,  
 6525 ED Nijmegen, The Netherlands

(Received 26 May 1998)

Rotationally resolved spectra of the  $b^1\Sigma_g^+(v=0) \leftarrow X^3\Sigma_g^-(v=0)$  band of molecular oxygen are recorded by cavity-ring-down (CRD) spectroscopy in magnetic fields up to 20 T. Measurements are performed in a 3-cm-long cavity, placed in the homogeneous field region inside a Bitter magnet. CRD absorption spectra are measured with linearly and circularly polarized light, leading to different  $\Delta M$  selection rules in the molecular transition, thereby aiding in the assignment of the spectra. Dispersion spectra are obtained by recording the rate of polarization rotation, caused by magnetic circular birefringence, using the polarization-dependent CRD detection scheme. Matrix elements for the Hamiltonian and for the transition moment are presented on a Hund's case  $a$  basis in order to calculate the frequencies and intensities of the rotational transitions of the oxygen A band in a magnetic field. All spectral features can be reproduced, even in the highest magnetic fields. The molar magnetic susceptibility of oxygen is calculated as function of the magnetic-field strength and the temperature, and a discussion on the alignment of the oxygen molecules in the magnetic field is given. [S1050-2947(98)06710-9]

PACS number(s): 33.55.Be, 33.15.Kr, 33.70.-w, 39.30.+w

### I. INTRODUCTION

The  $b^1\Sigma_g^+ \leftarrow X^3\Sigma_g^-$  magnetic dipole transition of molecular oxygen is very important in molecular spectroscopy. Especially the  $b^1\Sigma_g^+(v=0) \leftarrow X^3\Sigma_g^-(v=0)$  band (the A band) is well studied for remote sensing applications in the atmosphere [1,2], since the system lies in a relatively transparent part of the atmospheric spectrum. Although this transition is spin forbidden, it becomes weakly magnetic dipole allowed due to a rather large spin-orbit coupling between the  $b^1\Sigma_g^+$  state and the lowest spin component of the  $X^3\Sigma_g^-(M_S=0)$  state [3].

The A band of  $^{16}\text{O}_2$  has been used to test the symmetrization postulate for spin-0 nuclei [4,5]. Since the nuclear-spin of  $^{16}\text{O}$  is zero, the nuclear-spin function of  $^{16}\text{O}_2$  is symmetric. Furthermore, the vibrational wave function is symmetric under the exchange of the nuclei. Since the total wave function must be symmetric, only rotational states with even (odd) rotational quantum number  $N$  are therefore allowed if the electronic wave function is symmetric, e.g., the  $b^1\Sigma_g^+$  state (antisymmetric, e.g., the  $X^3\Sigma_g^-$  state). In order to test the symmetrization postulate, Angelis *et al.* [4] and Hilborn and Yuca [5] used sensitive diode laser absorption spectroscopy to search for the forbidden states, i.e., to search for transitions arising from even  $N$  in the  $X^3\Sigma_g^-$  state. They set an upper limit of about  $6 \times 10^{-7}$  to a possible violation of this postulate. Several groups are trying to improve the detection sensitivity on the oxygen A band. Besides direct absorption spectroscopy, techniques like cavity-ring-down (CRD) and magnetic rotation spectroscopy (MRS) offer promising perspectives [6,7]. Recently, several MRS studies on the A band have been reported [7-9]. Since the line profiles in MRS spectra are combinations of absorption and dispersion curves, the line profiles are rather complicated. In

order to be able to extract quantitative information from the MRS spectra, detailed information on the frequency shifts and rotational line intensities as functions of the magnetic field is required.

Magnetic trapping of atoms has led to a breakthrough in various fields of research, e.g., the creation of Bose-Einstein condensates [10] and "laserlike" atoms [11]. In principle, paramagnetic molecules can be trapped as well. The magnetic field splits and shifts the energy levels of the molecule as a result of the interaction between the magnetic dipole moment and the magnetic field. A molecule in a state with a positive Zeeman shift, i.e., in a state that increases in energy with increasing magnetic field, will be attracted toward a field minimum when placed in an inhomogeneous magnetic field. Doyle *et al.* [12] described a method for loading paramagnetic atoms and molecules into a magnetic trap (which consists of two coils in an anti-Helmholtz configuration). Recently, they demonstrated this method by trapping atomic europium [13]. Molecular oxygen is thought to be a promising candidate for trapping molecules [12]. Laser spectroscopy on the A band of oxygen can be used as a probe in order to determine the number density and rotational temperature of the trapped molecules. In order to interpret the recorded spectra, a detailed knowledge of the frequencies and intensities of the rotational lines as a function of the magnetic-field strength is a prerequisite.

Recently, we reported on polarization dependent cavity ring down (PD-CRD) spectroscopy, [14] a spectroscopic technique which combines the advantages of MRS and CRD spectroscopy. In this technique the *rate of polarization rotation* of the light is measured rather than the rate of absorption in CRD spectroscopy or the total polarization rotation in MRS. We demonstrated the PD-CRD technique in a study of the magneto-optical effects in molecular oxygen [14]. In a magnetic field perpendicular to the axis of the ring-down

cavity (Voigt configuration), the absorption spectrum due to magnetic dichroism of the  $b^1\Sigma_g^+(v=2) \leftarrow X^3\Sigma_g^-(v=0)$  transition of  $O_2$  was measured. In a magnetic field parallel to the cavity axis (Faraday configuration), the dispersion spectrum due to magnetic circular birefringence was measured. In this work [14] the highest possible magnetic field in the Faraday configuration was only 0.02 T, which was too small to resolve the dispersion curves of the individual Zeeman components. In the present experiment, the magnetic fields are sufficiently high that fully resolved dispersion spectra can be recorded.

In this paper, the rotationally resolved absorption spectra of the A band of molecular oxygen measured in magnetic fields up to 20 T by the CRD method are presented. The observed shifts and splittings of the rotational lines induced by the magnetic field are solely a result of the shifts and splittings of the rotational levels in the  $X^3\Sigma_g^-(v=0)$  state, since the rotational levels of the  $b^1\Sigma_g^+$  state are not affected by the magnetic field. In other words, the recorded spectra as function of the magnetic field directly visualize the magnetic-field dependence of the rotational energy levels of the  $X^3\Sigma_g^-$  state. The CRD experiments have been performed with left- and right-hand circularly polarized light, and it is explicitly demonstrated that the polarization state of the light is hardly affected by the multiple reflections on the mirrors. A detailed theoretical description is presented which explains all observed spectral features, and which will be valuable for future experiments on oxygen. Although the applied magnetic fields in MRS (and also in PD-CRD spectroscopy) are generally much weaker than 20 T, the spectra in high fields show that the theoretical description used to explain the low-field spectra is still valid.

This theoretical description gives us the possibility to look at physical effects which are a result of the interaction between the oxygen molecules and the magnetic field. First, the spin contribution to the molar magnetic susceptibility of oxygen is calculated as function of the magnetic-field strength and the temperature, and is compared to Curie's law. Furthermore, in a high magnetic field the oxygen molecule might be in a so-called pendular state. In a (magnetic) pendular state, the molecular magnetic dipole moment librates about the field direction as a result of its interaction with the magnetic field [15,16], and the degree of alignment of  $O_2$  in a magnetic field is discussed.

## II. THEORY

This section provides the necessary theory to describe the energy levels, transition frequencies, and rotational line intensities of the  $b^1\Sigma_g^+ \leftarrow X^3\Sigma_g^-$  transition of molecular oxygen in a magnetic field. Concepts and notations provided by Watson [17] are used. We start with the Hamiltonians of oxygen in the absence of an external magnetic field.

The effective rotational Hamiltonian in the  $b^1\Sigma_g^+$  state is

$$H' = B' \mathbf{J}^2, \quad (1)$$

where  $\mathbf{J}$  is the total angular momentum. The rotational constant  $B'$  is an effective constant since it contains effects of the Van Vleck transformation needed to eliminate terms in the Hamiltonian which couple different electronic states. The

energy eigenvalues of Eq. (1) are given by  $B'J(J+1)$  and corresponding eigenfunctions by

$$|0, J, M\rangle = |^1\Sigma_0^+\rangle |J, 0, M\rangle, \quad (2)$$

where the wave function is split into a spin factor and a symmetric-top wave function  $|J, K, M\rangle$  with  $K=0$ . The subscript 0 in the spin factor denotes the value of  $\Omega$ ; the  $g$ -subscript has been dropped for clarity (*vide infra*). For a correct description of the  $b^1\Sigma_g^+$  state the centrifugal distortion term should be included in the Hamiltonian [Eq. (1)]. Values for the molecular constants can be found in Refs. [2,6].

The effective spin-rotation Hamiltonian for the  $X^3\Sigma_g^-$  state is

$$H'' = B'' \mathbf{N}^2 + \gamma \mathbf{N} \cdot \mathbf{S} + \frac{2}{3} \lambda (3S_z^2 - \mathbf{S}^2), \quad (3)$$

where  $\mathbf{N} = \mathbf{J} - \mathbf{S}$  is the rotational angular momentum, and  $\mathbf{S}$  the total electronic spin.  $B''$  is an effective rotational constant,  $\gamma$  ( $\mu_0$  in Refs. [18,19]) the spin-rotation interaction constant, and  $\lambda$  the spin-spin interaction constant. For  $^{16}O_2$  these constants are [19]  $B'' = 1.4377$ ,  $\gamma = -8.4 \times 10^{-3}$ , and  $\lambda = 1.9848 \text{ cm}^{-1}$ , and  $B''$  and  $\lambda$  are thus of the same order of magnitude. A discussion about the Van Vleck transformation for this state can be found in the work of Tinkham and Strandberg [20]. Expressions for a more complete Hamiltonian including higher-order effects can be found in Refs. [18,19].

Ground-state energy levels can be found by a diagonalization of the pure triplet Hamiltonian of Eq. (3). The coupling scheme for the angular momenta in the  $X^3\Sigma_g^-$  state of  $O_2$  is close to Hund's case (b). However, the calculation of the transition probabilities of rotational transitions in the  $b^1\Sigma_g^+ \leftarrow X^3\Sigma_g^-$  system is simplified if the Hund's case (a) coupling scheme is used. The Hund's case (a) basis functions, in which the eigenfunctions of Eq. (3) can be expressed, are [17]

$$|\Omega, J, M\rangle = |^3\Sigma_\Omega^-\rangle |J, \Omega, M\rangle, \quad \Omega = -1, 0, 1. \quad (4)$$

The  $K$  value of the symmetric top wave function is matched to the value of  $\Omega$ . On this basis set, the Hamiltonian blocks in  $3 \times 3$  matrices belonging to the different  $J$  values (except for  $J=0$ ). The matrix elements can be evaluated after choosing the phases of the rotational and spin functions. Following the choice of Watson [17],

$$(J_x \pm iJ_y) |J, K, M\rangle = [J(J+1) - K(K \mp 1)]^{1/2} |J, K \mp 1, M\rangle \quad (5)$$

and

$$(S_x \pm iS_y) |^3\Sigma_\Omega^-\rangle = [2 - \Omega(\Omega \mp 1)]^{1/2} |^3\Sigma_{\Omega \pm 1}^-\rangle, \quad (6)$$

the matrix elements can be evaluated. For a given  $J$  the energy levels and the eigenfunctions are obtained after diagonalization of the matrix. The three levels can be labeled with  $N$ , a good quantum number provided that the  $X^3\Sigma_g^-$  state of  $O_2$  can be described as pure Hund's case (b). In increasing energy order the levels are labeled with  $N=J-1$ ,  $N=J$ , and  $N=J+1$ .

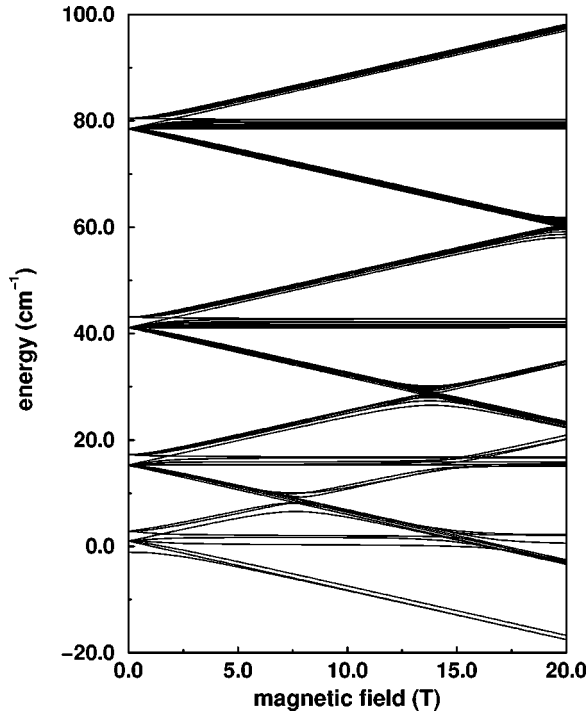


FIG. 1. Energy-level diagram of the  $X^3\Sigma_g^-(v=0)$  state of molecular oxygen as function of the magnetic field. The zero at the energy axis is taken at the hypothetical level  $N=J=0$  [18].

Since for  $O_2$  the spacing between the levels with different  $N$  values is much larger than the spacing between the  $J$  levels, the energy-level structure in the  $X^3\Sigma_g^-$  state shows groups of three levels in which the group is labeled by  $N$  and the three levels with  $J$ . As discussed in Sec. I, levels with  $N$  even do not exist in the  $X^3\Sigma_g^-$  state of  $^{16}O_2$ , while in the  $b^1\Sigma_g^+$  state, where  $N=J$ , levels with  $N$  odd do not exist due to spin-statistical considerations. Transitions between rotational levels ( $N'', J''$ ) in the  $X^3\Sigma_g^-(v=0)$  state and rotational levels ( $N', J'$ ) in the  $b^1\Sigma_g^+(v=0)$  state are denoted as  $\Delta N \Delta J(N'', J'')$ , where  $\Delta N = N' - N''$  and  $\Delta J = J' - J''$  are denoted as  $O, P, Q, R,$  and  $S$  for a change in quantum number of  $-2, -1, 0, 1, 2,$  respectively.

If an external magnetic field is applied, an extra term in the Hamiltonians of the ground and excited state has to be added to describe the interaction of the molecule with the magnetic field. For the  $b^1\Sigma_g^+$  state, however, this term can be neglected since both  $S$  and  $\Lambda$  are 0. For the  $X^3\Sigma_g^-$  state, the dominant contribution is due to the interaction between the electronic spin magnetic moment and the external field  $\mathbf{H}$ ,

$$H_{\text{int}} = g_s \beta \mathbf{S} \cdot \mathbf{H} = g_s \beta S_Z H, \quad (7)$$

in which  $g_s = 2.00232$  is the  $g$  factor of the free-electron spin, and  $\beta$  is the Bohr magneton. In the last step it is assumed that the magnetic field only has a component along the  $Z$  axis (note that the space-fixed axis system is denoted by  $X, Y, Z$ , and the molecule-fixed axis system by  $x, y, z$ ).

In order to calculate the energies of the rotational levels, the matrix elements of  $S_Z$  on a Hund's case (a) basis are needed. They can be evaluated using Eq. (6) and the matrix elements of the direction cosines, and are given in the Ap-

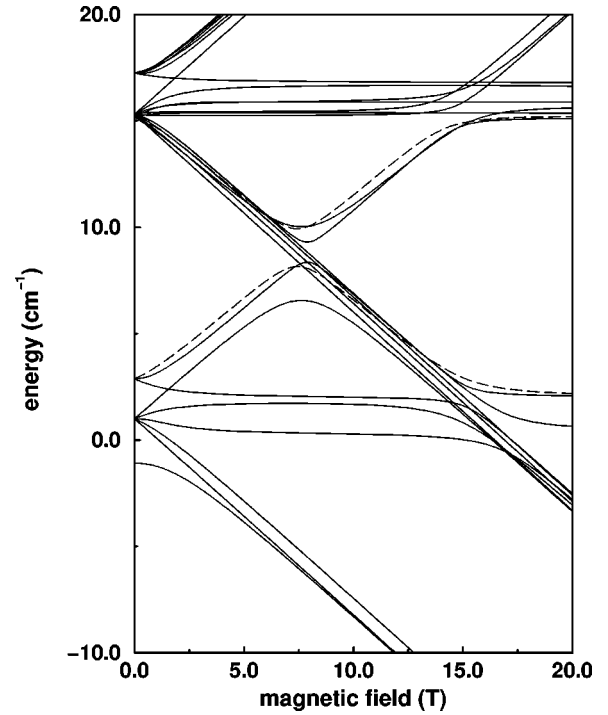


FIG. 2. Part of the energy-level diagram of the  $X^3\Sigma_g^-(v=0)$  state of molecular oxygen as a function of the magnetic field. The zero at the energy axis is taken at the hypothetical level  $N=J=0$  [18]. The  $N=1, J=1, M=+1$  (lower), and  $N=3, J=2, M=+1$  levels are dashed. The mixing coefficients of their wave functions are shown in Fig. 10.

pendix. For the actual calculation, we have used as basis the eigenfunctions of oxygen in zero magnetic field:

$$|N, J, M\rangle = c_{NJ}^{-1} |1, J, M\rangle + c_{NJ}^0 |0, J, M\rangle + c_{NJ}^1 |1, J, M\rangle. \quad (8)$$

This has the advantage that on the diagonal of the matrix the energies of the rotational levels in zero magnetic field appear, which have been directly taken from Table 10 of Ref. [18]. Eigenfunctions up to and including  $N=31$  have been used to set up the matrix of the Hamiltonian in a magnetic field (giving a  $48 \times 48$  matrix, since only odd  $N$  exist). An additional advantage of using this basis rather than a pure Hund's case (a) basis is that the eigenvectors directly provide the mixing coefficients of the field-free rotational levels due to the presence of the magnetic field.

The energy-level structure in the  $X^3\Sigma_g^-(v=0)$  state as function of the magnetic field is shown in Figs. 1 and 2. At zero magnetic field, the levels with the same  $N$  value group together and are labeled with  $J=N-1, J=N+1,$  and  $J=N$  in increasing energy order. It is clearly seen that the energy difference between  $J=N-1$  and  $J=N+1$  rapidly decreases as function of  $N$ . Turning on the magnetic field results in a splitting of each  $(N, J)$  level in  $(2J+1)$   $M$  components. After a somewhat chaotic part in which the energy levels interact strongly with each other (below 2.5 T), the levels within a  $N$  multiplet regroup into three components which relative energy can be described with

$$\Delta E_{\text{int}} = g_s \beta M_S H \approx 0.9 M_S H \quad (\text{cm}^{-1}), \quad (9)$$

with  $M_S = -1, 0, \text{ and } 1$ , and  $H$  in T. This is the molecular analog of the Paschen-Back effect, where for high fields  $\mathbf{S}$  couples to the field [21].

In deriving the effective Hamiltonians [Eqs. (1) and (3)], a Van Vleck transformation has been used to remove the coupling terms describing the interaction between different electronic states. The same transformation has to be applied to the magnetic dipole moment operator in order to obtain an effective operator  $\mathbf{M}$  which couples the  $b^1\Sigma_g^+$  and  $X^3\Sigma_g^-$  states via a magnetic dipole transition. By taking into account rotational symmetry about the molecular axis, reflection symmetry of the  $\Sigma$  state, and time-reversal arguments, Watson [17] showed that the only nonvanishing real magnetic dipole moment  $\mathcal{M}$  is given by

$$\begin{aligned} & \langle ^1\Sigma_0^+ | 2^{-1/2}(M_x + iM_y) | ^3\Sigma_1^- \rangle \\ &= \langle ^1\Sigma_0^+ | 2^{-1/2}(M_x - iM_y) | ^3\Sigma_1^- \rangle = \mathcal{M}. \end{aligned} \quad (10)$$

The (relative) rotational lines strengths can now be calculated by evaluating  $\langle \Psi' | M_I | \Psi'' \rangle$ , in which  $\Psi'$  and  $\Psi''$  are the eigenfunctions in, respectively, the  $b^1\Sigma_g^+$  and  $X^3\Sigma_g^-$  state, and  $M_I$  is a space-fixed component of the (molecule-fixed) transition moment. In the experiments described in this paper, the light exciting the molecules travels along the direction of the magnetic field (which is along the  $Z$  axis). If the polarization is linear, the matrix elements have to be evaluated for  $M_I = M_x$ . If the light is circularly polarized, the matrix elements for  $M_I = M_+$  or  $M_-$  are required [where  $M_+ = 2^{-1/2}(M_x + iM_y)$  and  $M_- = 2^{-1/2}(M_x - iM_y)$ ]. These matrix elements are given in the Appendix.

### III. EXPERIMENTAL SETUP

A schematic representation of the experimental setup is depicted in Fig. 3. Since the magnetic field is homogeneous over a few centimeters, a very short ring-down cavity has been used in order to prevent that the spectra become too complex. The length of the cavity is chosen such that the broadening of the rotational lines due to the inhomogeneity of the magnetic field is comparable to the combination of Doppler and pressure broadening. The ring-down cavity is formed by two planoconcave mirrors with a diameter of 25 mm and a radius of curvature of  $-1$  m, placed 3 cm apart. The mirrors are coated for an optimum reflectivity at 810 nm, with a quoted reflectivity of better than 0.9999 (Newport, SuperMirrors). The time constant  $\tau$  that describes the decay of the light in the empty cavity in our setup is around 350 ns, corresponding to an effective absorption path length of 105 m (for one  $\tau$ ) and an effective reflection coefficient of  $R \approx 0.9997$  in the spectral region of the  $0 \leftarrow 0$  transition of the atmospheric band of molecular oxygen around 762 nm. The decay constant of the empty cavity is independent of the applied magnetic field.

The mirrors are mounted on a short tube, in a fixed position relative to each other. This short cavity is placed inside an 84-cm-long cell, which is inserted in a Bitter magnet with a bore of 3.1 cm. The axis of the cavity is parallel to the magnetic-field lines (Faraday configuration). The cavity is positioned in the center of the magnet in a region where the field is rather homogeneous; the field at the position of the mirrors drops to 98.5% of the maximum field at the center of

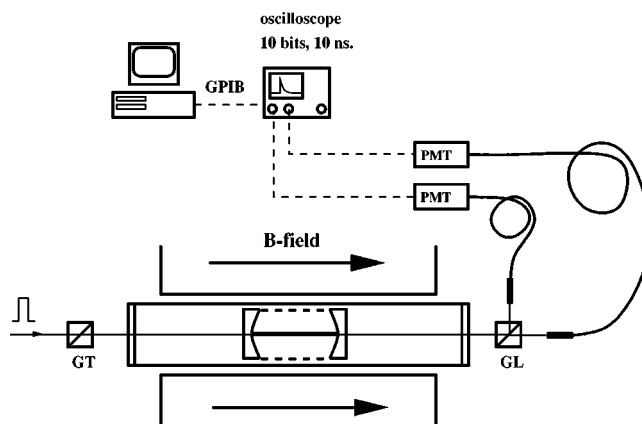


FIG. 3. Scheme of the experimental setup. The CRD cavity consists of two high reflectance mirrors with a separation of 3 cm. This cavity is placed inside an 84-cm-long cell, which is inserted in a Bitter magnet (bore 3.1 cm). For PD-CRD a Glan-Thompson (GT) polarizer is placed in front of the entrance window of the cell, and a Glan-Laser (GL) analyzer is used to split the light exiting the cell into two orthogonal polarization directions. Each component is focused onto a fiber which is coupled to a photomultiplier tube (PMT). For ‘‘conventional’’ CRD the Glan-Laser analyzer is removed, and, optionally, a  $\lambda/4$  plate is placed between the Glan-Thompson polarizer and the entrance window of the cell to create circularly polarized light.

the cavity. The long cell is made of a stainless-steel tube which is closed off by two borosilicate Crown Glass windows. The cell is filled with pure molecular oxygen (100–500 mbar), and holes in the small ring down cavity tube allow the oxygen to enter the cavity as well.

Pulsed-laser radiation at a wavelength of 762 nm is obtained from a Nd:YAG (yttrium aluminum garnet) laser pumped dye laser (Spectra Physics GCR-150–10 PDL-3 combination, 10-Hz repetition rate, 5-ns duration pulses), delivering pulses with several mJ of energy in a spectral profile with a bandwidth of approximately  $0.07 \text{ cm}^{-1}$ . Prior to entering the cell with the ring-down cavity, the incoming laser beam passes through a Glan-Thompson polarizer with an extinction of  $10^{-5}$ . For the PD-CRD experiments, the light exiting the ring down cavity is passed through a Glan-Laser polarizer, and split into its two mutually orthogonally polarized components (extinction of  $10^{-5}$ ). The axis of this Glan-Laser analyzer can be oriented relative to the polarization direction of the incoming beam with an accuracy of  $0.1^\circ$ . Since the photomultiplier tubes (PMT’s) cannot be placed in the neighborhood of the Bitter magnet, the light is coupled into 13-m-long fibers which are connected to the PMT’s.

The signals of both PMT’s are amplified and displayed on a fast (10 ns) and high-resolution (ten bit) digital oscilloscope (LeCroy 9430). At every wavelength position about 20 transients, every transient recorded over a  $5\text{-}\mu\text{s}$  duration time interval, is summed on the 16-bit on-board memory of the oscilloscope and read out by a personal computer via a GPIB interface connection. The characteristic ring down time  $\tau$  is determined by fitting the natural logarithm of the data to a straight line, using a weighted least-squares fitting algorithm. Dispersion spectra are obtained by plotting the difference between the cavity loss rates ( $1/c\tau$ ) for the two polarization directions as a function of wavelength [14].

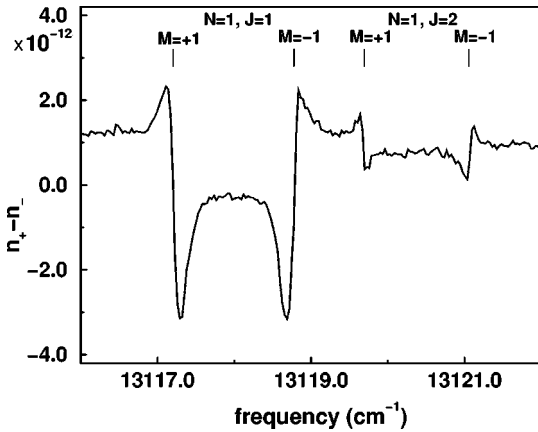


FIG. 4. PD-CRD dispersion spectrum in the region of the  ${}^P P(1,1)$  transition. Measurements are performed with 200 mbar of oxygen in a magnetic field of 1.5 T. The magnetic field splits the transition into two components. The two small dispersion curves belong to the  ${}^P O(1,2)$  transition, which becomes allowed through a magnetic field induced mixing with the  ${}^P P(1,1)$  transition. The dispersion curves are labeled with the quantum numbers of the  $X^3\Sigma_g^-$  state.

In order to perform ‘‘conventional’’ CRD spectroscopy, [22,23] the Glan-Laser analyzer is removed, and all light exiting the cavity is focused onto the fiber which is connected to a PMT. Optionally, by placing a  $\lambda/4$  plate between the Glan-Thompson polarizer and the entrance window of the cell, circularly polarized light is created.

## IV. RESULTS AND DISCUSSION

### A. PD-CRD spectra

In Fig. 4, a PD-CRD spectrum of the  ${}^P P(1,1)$  transition of molecular oxygen is shown, measured on 200-mbar oxygen in a magnetic field of 1.5 T. The magnetic field splits the  $(N=1, J=1)$  level in the  $X^3\Sigma_g^-(v=0)$  state into three components labeled with  $M = -1, 0,$  and  $+1$ . Since the selection rules in the Faraday configuration are  $\Delta M = \pm 1$ , only two transitions can be made to the  $(N=0, J=0)$  level in the  $b^1\Sigma_g^+(v=0)$  state. It is evident that the spectrum of Fig. 4 can be obtained by subtraction of two dispersion curves centered at the position of the two transitions, as we described previously [14]. At higher frequencies two weaker dispersion curves are visible in Fig. 4, which arise from the  ${}^P O(1,2)$  transition. In the absence of the magnetic field this transition is forbidden since  $\Delta J = -2$ . However in a magnetic field of 1.5 T the eigenfunction of the ground-state level denoted with  $(N=1, J=2)$  has 10%  $(N=1, J=1)$  character, and the  ${}^P O(1,2)$  transition thereby gains intensity. Therefore, it is expected that the intensity ratio of the  ${}^P P(1,1)$  and  ${}^P O(1,2)$  dispersion curves is 9:1. However, the intensity of the measured  ${}^P P(1,1)$  dispersion curve is underestimated because the bandwidth of the laser is only slightly smaller than the linewidth of the dispersion curves [23]. The steps in the baseline of the spectrum are due to nearby transitions which still have a significant contribution in the region of the  ${}^P P(1,1)$  line, since dispersion curves extend over large spectral regions.

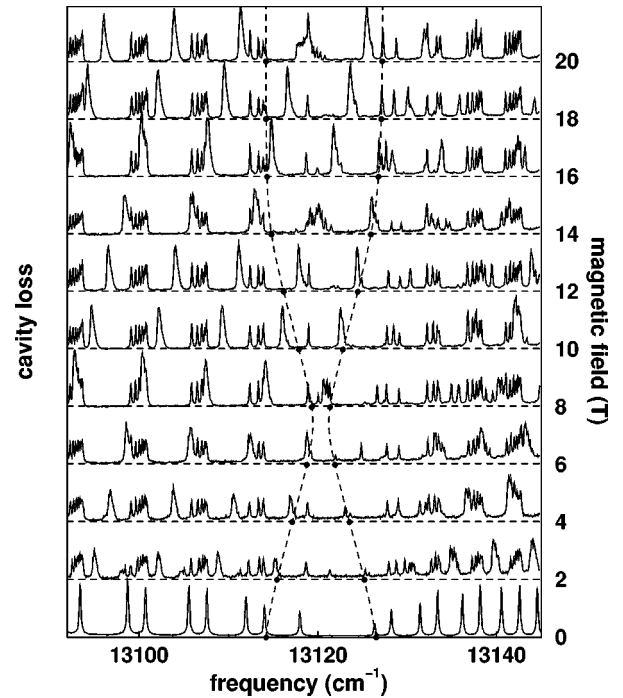


FIG. 5. CRD spectrum of the central part of the  $b^1\Sigma_g^+(v=0) \leftarrow X^3\Sigma_g^-(v=0)$  transition of molecular oxygen as function of the magnetic field (in T). Right-hand circularly polarized ( $\sigma^+$ ) light has been used to excite the molecules. The vertical scale is the same for each spectrum, and has been omitted for clarity (see Fig. 9). The spectrum measured in the absence of a magnetic field is recorded under different experimental conditions, in order to show the correct line intensities. The transitions from the  $N=1, J=1,$  and  $M = +1$  level (around  $13\,125\text{ cm}^{-1}$ ) and  $N=3, J=2,$  and  $M = +1$  level of the  $X^3\Sigma_g^-(v=0)$  state toward the  $N'=J'=2$  and  $M' = +2$  level of the  $b^1\Sigma_g^+(v=0)$  state are indicated by the dashed lines. The energy and the mixing coefficients of the wave functions of both ground-state levels are shown, respectively, in Figs. 2 and 10.

### B. CRD spectra

CRD spectra of oxygen have been recorded with linear, right-hand circularly polarized, and left-hand circularly polarized light as functions of the magnetic field. Figure 5 shows the spectra for right-hand circularly polarized light ( $\sigma^+$ ), containing only transitions with  $\Delta M = +1$ . Only the central part of the  $b^1\Sigma_g^+(v=0) \leftarrow X^3\Sigma_g^-(v=0)$  transition is displayed. Three different kinds of spectral features can be distinguished. First, there are features which remain (almost) at the same frequency while increasing the magnetic field. Second, there are features which shift with approximately  $0.9\text{ cm}^{-1}/\text{T}$  to higher frequency. Third, there are features which appear and disappear as the magnetic field increases. The latter features are mainly located in the central part of the spectra ( $13\,118\text{--}13\,119\text{ cm}^{-1}$ ). Figure 6 shows the spectra for left-hand circularly polarized light ( $\sigma^-$ ), containing only transitions with  $\Delta M = -1$ . Again the same three spectral features can be distinguished, although the features which shift as function of the magnetic field now shift to lower frequency. The CRD spectra measured with linear polarized light contain transitions with  $\Delta M = \pm 1$  and are not shown here, since they can be obtained by direct summation of the spectra measured with right- and left-handed circularly polarized light (*vide infra*).

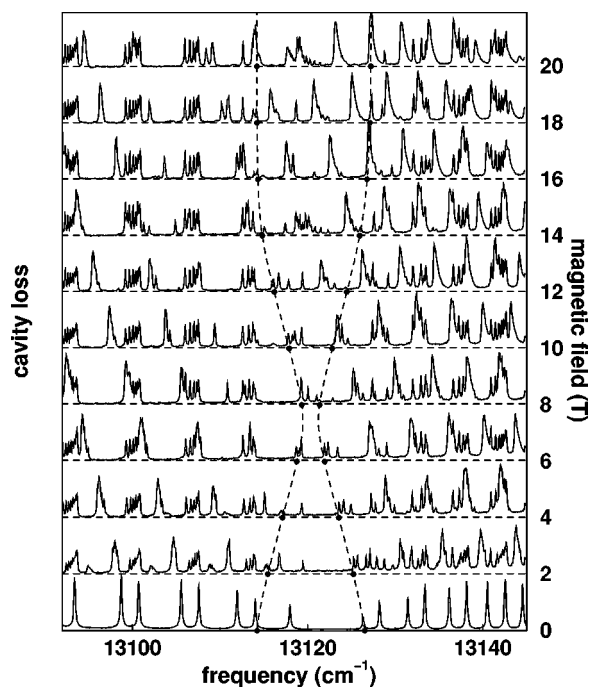


FIG. 6. CRD spectrum of the central part of the  $b^1\Sigma_g^+(v=0) \leftarrow X^3\Sigma_g^-(v=0)$  transition of molecular oxygen as function of the magnetic field (in T). Left-hand circularly polarized ( $\sigma^-$ ) light has been used to excite the molecules. The vertical scale is the same for each spectrum, and has been omitted for clarity (see Fig. 9). The spectrum measured in the absence of a magnetic field is recorded under different experimental conditions, in order to show the correct line intensities. The transitions from the  $N=1, J=1$ , and  $M=+1$  level (around  $13125\text{ cm}^{-1}$ ) and  $N=3, J=2$ , and  $M=+1$  level of the  $X^3\Sigma_g^-(v=0)$  state toward the  $N'=J'=2$  and  $M'=0$  level of the  $b^1\Sigma_g^+(v=0)$  state are indicated by the dashed lines. The energy and the mixing coefficients of the wave functions of both ground-state levels are shown, respectively, in Figs. 2 and 10.

Comparing the spectra from Figs. 5 and 6 shows that the polarization state of the light inside the cavity remains well defined, since there exist strong features that are present in the  $\sigma^+$  spectra and that are totally absent in the  $\sigma^-$  spectra (and vice versa). Therefore, it is concluded that CRD spectroscopy can well be performed with (circularly) polarized light, which thereby can be used to simplify spectra.

Figure 7 shows the CRD spectra at 20 T measured with  $\sigma^+$ ,  $\sigma^-$ , and linearly polarized light. In addition, the sum of the  $\sigma^+$  and  $\sigma^-$  spectra (divided by 2) is shown. This sum spectrum should be identical to the spectrum measured with linearly polarized light, but, although all features can be found in both spectra, it is seen that the intensity of strong features which arise *solely* from  $\Delta M=+1$  or  $\Delta M=-1$  transitions are underestimated in the measured spectrum. This is an experimental artifact that can be understood as follows. The linearly polarized light can be decomposed into an equal amount of  $\sigma^+$  and  $\sigma^-$  polarized light. If there is no absorption by the molecules in the cavity, the transient measured at the exit of the cavity consists of the sum of two ( $\sigma^+$  and  $\sigma^-$ ) transients with the same decay time, and is a single exponentially decaying curve. Suppose the laser frequency is centered on a  $\Delta M=+1$  transition. Only the  $\sigma^+$  light can be absorbed in this case. Therefore, the decay time of the  $\sigma^+$  light in the cavity will be shorter than the

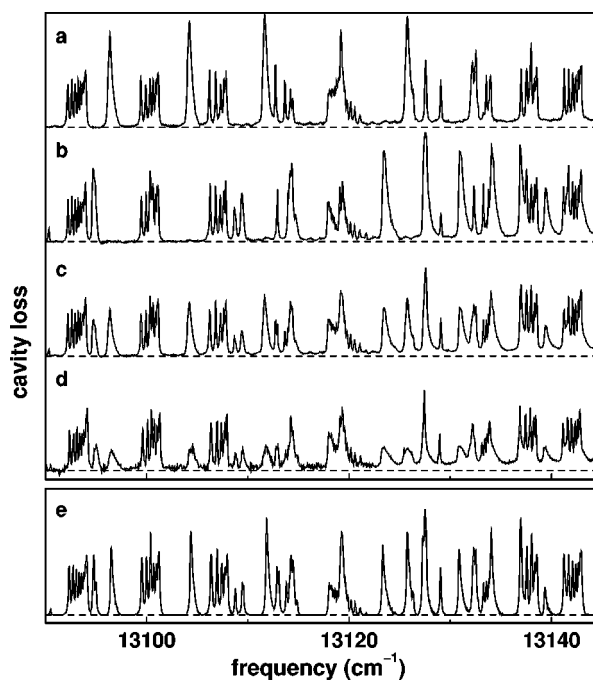


FIG. 7. CRD spectra of molecular oxygen at 20 T: the measured spectrum with  $\sigma^+$  polarized light (a), the measured spectrum with  $\sigma^-$  polarized light (b), the sum of the spectra shown in (a) and (b) divided by 2 (c), the measured spectrum with linearly polarized light (d), and the simulation of the spectrum with linearly polarized light (e). The vertical scale is the same for each spectrum, and has been omitted for clarity (see Fig. 9).

decay time of the  $\sigma^-$  light. Now the transient measured at the exit of the cavity is a sum of two transients with different decay times, and is no longer a single exponentially decaying curve. In the measurement procedure all transients are fit to a single exponential curve, and therefore the decay time will be overestimated (and thus the absorption will be underestimated). In Fig. 8, a calculation of this effect is shown. The observed absorption, i.e., the absorption deduced from the ring-down transient, is calculated as function of the real absorption. The biexponential transient has been fit using our standard weighted least-squares fitting algorithm, using a time window of three times the decay time in the absence of absorption. If the absorption is very strong, all the light of one polarization component is absorbed, and the decay time of the unabsorbed component is observed (being the decay of the empty cavity). No absorption is measured in that case. It is seen that there are already deviations at an absorption of 5% of the cavity losses of an empty cavity. It is therefore concluded that care has to be taken in the interpretation of the data recorded with linearly polarized light. This effect of underestimating the absorption is similar to the case of measuring a spectral feature with a spectral width which is smaller than the linewidth of the laser [23]. In that case, only part of the light that is coupled into the cavity is absorbed, and the recorded transient is a multiexponentially decaying curve. Note that the present effect is also present, however, when the laser linewidth is infinitely small.

With the theory presented in Sec. II, we have simulated the spectra at all magnetic fields. Examples are shown in Figs. 7(e) and 9. It is seen that the strongest transitions are underestimated. This is due to the linewidth effect [23], since

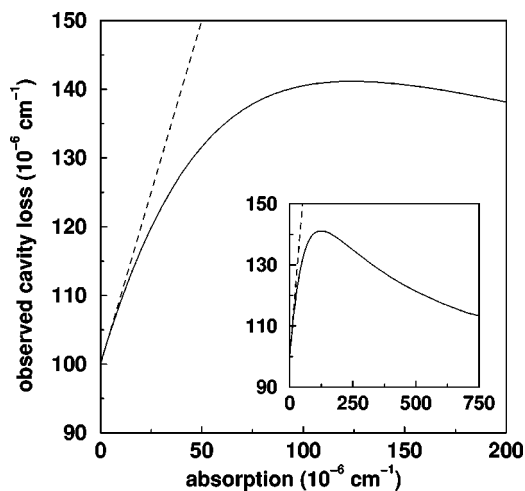


FIG. 8. When CRD spectroscopy in a magnetic field is performed with linear polarized light, absorptions induced by  $\sigma^+$  or  $\sigma^-$  light are underestimated. The horizontal axis shows the real absorption, the vertical axis the measured cavity losses. The vertical offset at zero absorption is caused by the cavity losses of the empty cavity. The value of the observed cavity losses is determined by fitting a calculated ring down transient to a single exponential decay, using a time window of three times the decay time if there is no absorption. Using a smaller time window would give smaller deviations between the observed and the real absorption.

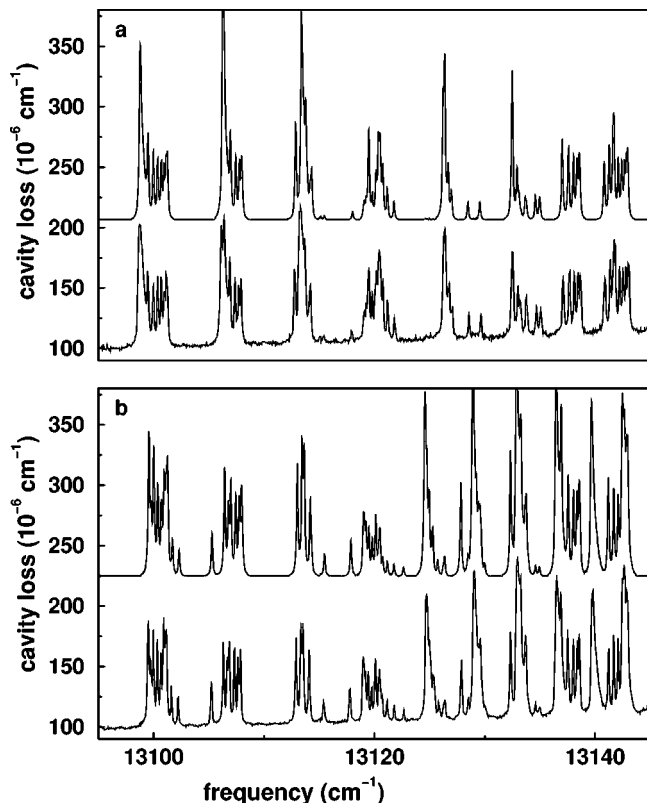


FIG. 9. Experimental and simulated (upper trace) spectra of oxygen in a magnetic field of 14 T measured with  $\sigma^+$ - (a) and  $\sigma^-$ - (b) polarized light. For clarity, the calculated spectra are shifted upwards.

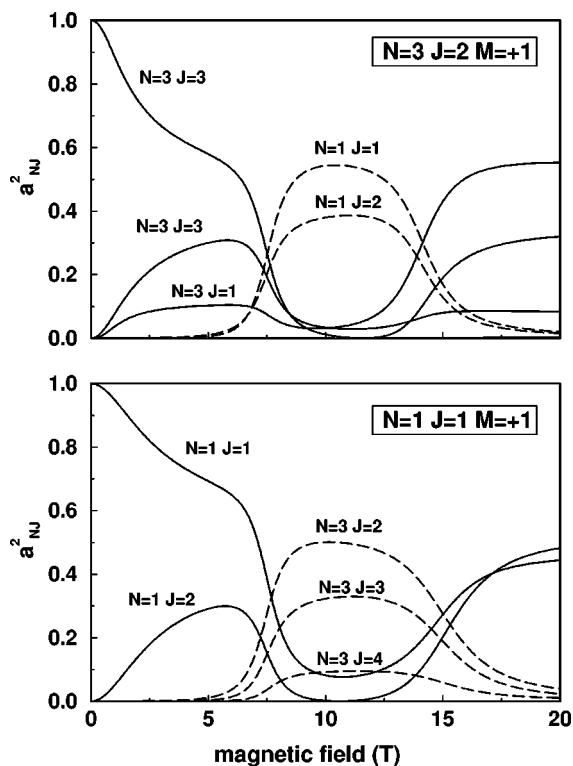


FIG. 10. The amount of  $N, J$  character ( $a^2_{NJ}$ ) in the wave function of the  $N=1, J=1$ , and  $M=+1$  (lower panel) and  $N=3, J=2$ , and  $M=+1$  (upper panel) levels of the  $X^3\Sigma_g^-(v=0)$  state is plotted as a function of the magnetic field. Both levels are indicated in the energy-level diagram of Fig. 2. The transitions from these two levels towards the  $N'=J'=2, M'=+2$ , and  $M'=0$  levels of the  $b^1\Sigma_g^+(v=0)$  state are marked in the spectra of Figs. 5 and 6.

the linewidth of the laser is only slightly smaller than the linewidth of the rotational lines. The agreement between the simulated and experimental spectra is very good for all magnetic field strengths used. Since the energy levels in the  $b^1\Sigma_g^+$  state are not affected by the magnetic field, we can “project” the energy-level scheme onto the spectra. It is clearly seen that the features in Figs. 5 and 6 which are hardly affected by the magnetic field are described by Eq. (9) with  $M_S=0$ , and the features which shift are described by Eq. (9) with  $M_S=\pm 1$ .

The energy-level diagram of Fig. 1 shows also five perturbations (avoided crossings) at 8, 14 (three perturbations), and 20 T. These magnetic fields are just those where the spectra (Figs. 5 and 6) show the third kind of spectral features: the ones who appear and disappear. To illustrate the shifting of the lines, two transitions have been marked in Figs. 5 and 6: the  $^PQ(3,2)$  and  $^RQ(1,1)$  both originating from the  $M''=+1$  sublevel. Both transitions go to the same upper level ( $N'=J'=2$  and  $M'=+2$  in Fig. 5, and  $N'=J'=2$  and  $M'=0$  in Fig. 6), thus their relative frequency directly reflects the relative position of the ground-state energy levels which is shown in Fig. 2. Figure 10 shows the mixing of the wave functions of these levels as a function of the magnetic field. At low magnetic fields all  $J$  levels within one  $N$  multiplet interact with each other. At higher fields there is a strong interaction between the  $N=1$  and  $N=3$  multiplets, since their energy difference becomes smaller. At fields higher than 8 T the dominant character of both levels is

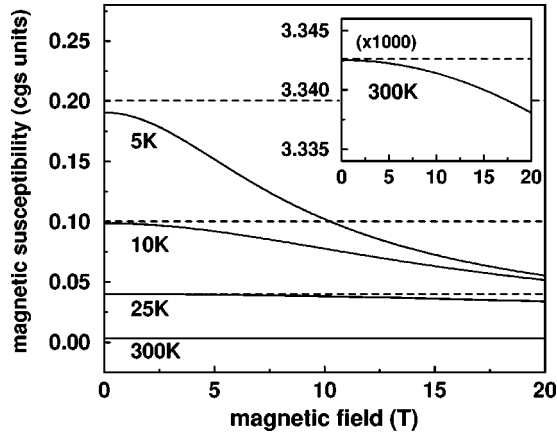


FIG. 11. The calculated spin part of the molar magnetic susceptibility ( $\chi_{\text{spin}}$ ) of molecular oxygen as function of the magnetic-field strength for various temperatures (solid lines). The dashed lines represent the values of  $\chi_{\text{spin}}$  calculated with Curie's law [Eq. (13)]. The inset shows  $\chi_{\text{spin}}$  at 300 K.

exchanged. At about 14 T both levels interact strongly with two other levels, resulting in a change of relative energy and in a change of the mixing coefficients.

### C. Magnetic susceptibility and alignment

Since both the frequencies and intensities of all rotational transitions of the  $b^1\Sigma_g^+ \leftarrow X^3\Sigma_g^-$  band can be described accurately with the theory of Sec. II, we can use this theoretical framework to calculate the spin contribution to the molar magnetic susceptibility. This spin part is the dominant contribution to the magnetic susceptibility. Although other parts (e.g., the diamagnetic term) contribute to the measured molar magnetic susceptibility as well, those contributions are in the order of a few parts per thousand at room temperature [20]. Following Van Vleck's classic work on susceptibilities [24], the spin part of the susceptibility can be obtained from the averaged magnetic dipole moment:

$$\chi_{\text{spin}} = \frac{N_0}{H} \frac{\sum_i \langle \mu_i \rangle e^{-E_i/kT}}{\sum_i e^{-E_i/kT}} \quad (11)$$

where  $N_0$  is the Avogadro number,  $H$  the magnetic field, the sum is taken over all energy levels  $i$  with energy  $E_i$ , and the expectation value of the magnetic dipole moment is given by

$$\langle \mu_i \rangle = \langle \Psi_i | (-g_s \beta S_z) | \Psi_i \rangle. \quad (12)$$

Usually the expression for  $\chi_{\text{spin}}$  is approximated by Curie's law [20,24]

$$\chi_{\text{spin}} = \frac{N_0 g_s^2 \beta^2 S(S+1)}{3kT}, \quad (13)$$

since evaluating Eq. (11) requires the exact energies and wave functions of all occupied energy levels. In Fig. 11 the calculated  $\chi_{\text{spin}}$  is shown as function of the magnetic-field strength for various temperatures using both the exact expression [Eq. (11), solid lines] and Curie's law (dashed

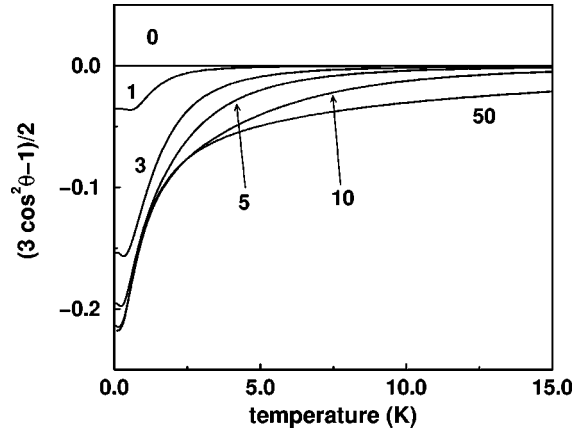


FIG. 12. Alignment of an ensemble of oxygen molecules as function of the temperature for a magnetic field of 0, 1, 3, 5, 10, and 50 T.

lines). From the figure it is seen that Curie's law can be applied well for high temperatures and low magnetic-field strengths. At low temperatures, where only a few rotational levels are populated, the deviation from Curie's law is substantial.

The molar magnetic susceptibility describes the magnetic response of the oxygen gas, and can be used to calculate the force exerted on the gas by an inhomogeneous magnetic field. However, it does not provide information on a possible alignment of the molecules in a magnetic field. The expectation value of  $\cos^2\theta$ , where  $\theta$  is the angle between the molecular axis and the external magnetic field, is used to describe the alignment of the molecule in a specific rotational level [25]. By averaging over all internal states that the molecules can be in, a measure for the alignment of the ensemble of oxygen molecules is obtained. If there is no alignment, the expectation value of  $\cos^2\theta$  is equal to  $\frac{1}{3}$ . In Fig. 12, the alignment parameter [25]  $(3 \cos^2\theta - 1)/2$  is plotted as function of the temperature for various magnetic fields. The temperature influences the alignment via the population distribution over the rotational levels.

Such an alignment was first reported by Slenczka, Friedrich, and Herschbach for jet-cooled ICl molecules, which were laser excited to the  $A^3\Pi_1$  state in a magnetic field of 0.8 T [16]. In their paper about the possibility of aligning paramagnetic molecules, Friedrich and Herschbach [15] explained that pure Hund's case (b) molecules in a state with  $\Lambda=0$  are not amenable to magnetic alignment, since neither the total electron spin  $\mathbf{S}$  nor the projection of the total electron angular momentum on the molecular axis  $\Lambda$  provides a grip on the molecular axis. The  $X^3\Sigma_g^-$  state of  $O_2$  has a large spin-spin interaction arising from the interaction of the magnetic dipole moments of the two unpaired electrons. This spin-spin interaction tends to align the spins along the internuclear axis as in Hund's case (a) [26]. Therefore, the  $X^3\Sigma_g^-$  state cannot be described as a pure Hund's case (b). In high magnetic fields  $\mathbf{S}$  couples to the field, and, due to the spin-spin interaction, the field gets a grip on the molecular axis. Thus several rotational states may become pendular states in high magnetic fields. The curves in Fig. 12 show that at low temperatures, which can be readily obtained in supersonic jet expansions, an appreciable alignment is predicted.



## V. SUMMARY

In this paper it is demonstrated that sensitive direct absorption spectroscopy can be applied via PD-CRD and CRD spectroscopy in short cavities in environments that are difficult to access, like inside a high-field magnet. PD-CRD spectroscopy has been used to record well-resolved dispersion spectra of the  $b^1\Sigma_g^+(v=0) \leftarrow X^3\Sigma_g^-(v=0)$  transition, the A band, of molecular oxygen. CRD spectra of the A band have been measured with linearly and circularly polarized light as function of the magnetic field. It is shown that the polarization state of the light is not (or hardly) affected by the mirrors of the cavity. Therefore, circularly polarized light can be used in the CRD setup to simplify the measured spectra. Care has to be taken in the interpretation of the results when linearly polarized light is used, as this might lead to a systematic underestimate of absorptions that are exclusively induced by left- or right-handed circularly polarized light. A theoretical description for calculating the transition frequencies and line intensities for the  $b \leftarrow X$  system of oxygen is given, and is shown to be valid for magnetic fields up to 20 T. It is shown that molecular oxygen can be aligned in such high magnetic fields. This is a nice example of a molecular system in which the alignment is caused by the spin-spin interaction via a coupling of the spin angular momentum to the magnetic-field direction.

## ACKNOWLEDGMENTS

The authors would like to thank André van Roij for his excellent technical assistance. This work was part of the research program of the ‘‘Stichting voor Fundamenteel Onderzoek der Materie (FOM),’’ which is financially supported by the ‘‘Nederlandse Organisatie voor Wetenschappelijk Onderzoek (NWO),’’ and receives direct support by NWO via PIONIER Grant No. 030-66-89.

## APPENDIX

In this appendix the matrix elements of  $S_Z$ ,  $M_X$ ,  $M_+$ , and  $M_-$  are presented on a Hund’s case (a) basis. The external magnetic field is taken along the Z axis. The matrix elements of the direction cosines have been obtained from Refs. [27,28]. This phase convention is consistent with Eq. (5) [17,27,29]. Note that only the basis functions  $|\Omega, J, M\rangle$ , with  $\Omega = -1, 0$ , and 1 exist.

The matrix elements for  $S_Z$  are

$$\langle \Omega, J, M | S_Z | \Omega, J, M \rangle = \frac{\Omega^2 M}{J(J+1)}, \quad (\text{A1})$$

$$\langle \Omega, J-1, M | S_Z | \Omega, J, M \rangle = \Omega \left[ \frac{(J^2 - M^2)(J^2 - 1)}{J^2(4J^2 - 1)} \right]^{1/2}, \quad (\text{A2})$$

$$\langle \Omega \pm 1, J, M | S_Z | \Omega, J, M \rangle = \frac{M}{[2J(J+1)]^{1/2}}, \quad (\text{A3})$$

$$\begin{aligned} \langle \Omega \pm 1, J-1, M | S_Z | \Omega, J, M \rangle \\ = \pm \left[ \frac{(J^2 - M^2)(J \mp \Omega)(J \mp \Omega - 1)}{2J^2(4J^2 - 1)} \right]^{1/2}. \end{aligned} \quad (\text{A4})$$

These expressions are identical to those given by Tinkham and Strandberg [20].

The matrix elements for the transition moments are

$$\langle 0, J, M \pm 1 | M_I | \Omega, J, M \rangle = C_I \left[ \frac{(J \mp M)(J \pm M + 1)}{4J(J+1)} \right]^{1/2}, \quad (\text{A5})$$

$$\begin{aligned} \langle 0, J+1, M \pm 1 | M_I | \Omega, J, M \rangle \\ = C_I \frac{\mp \Omega}{J+1} \left[ \frac{(J \pm M + 1)(J \pm M + 2)J(J+1)}{4(2J+1)(2J+3)} \right]^{1/2}, \end{aligned} \quad (\text{A6})$$

$$\begin{aligned} \langle 0, J-1, M \pm 1 | M_I | \Omega, J, M \rangle \\ = C_I \frac{\mp \Omega}{J} \left[ \frac{(J \mp M)(J \mp M - 1)J(J+1)}{4(2J-1)(2J+1)} \right]^{1/2} \end{aligned} \quad (\text{A7})$$

where  $\Omega$  can take the values  $-1$  and  $+1$ . If the light is linearly polarized, then  $M_I = M_X$  and  $C_X = \mathcal{M}/\sqrt{2}$  [note that  $\mathbf{M}$  is the magnetic dipole moment defined in Eq. (10), while  $M$  is a quantum number]. If the light is  $\sigma^+$  polarized, then  $M_I = M_+$ ,  $C_+ = \mathcal{M}$ , and only the upper signs are taken (only  $\Delta M = +1$  transitions). If the light is  $\sigma^-$  polarized, then  $M_I = M_-$  and  $C_- = \mathcal{M}$ , and only the lower signs are taken (only  $\Delta M = -1$  transitions).

- 
- [1] K. J. Ritter and T. D. Wilkerson, *J. Mol. Spectrosc.* **121**, 1 (1987), and references therein.
- [2] A. J. Phillips, F. Peters, and P. A. Hamilton, *J. Mol. Spectrosc.* **184**, 162 (1997), and references therein.
- [3] B. Minaev, O. Vahtras, and H. Ågren, *Chem. Phys.* **208**, 299 (1996).
- [4] M. de Angelis, G. Gagliardi, L. Gianfrani, and G. M. Tino, *Phys. Rev. Lett.* **76**, 2840 (1996).
- [5] R. C. Hilborn and C. L. Yuca, *Phys. Rev. Lett.* **76**, 2844 (1996).
- [6] H. Naus, A. de Lange, and W. Ubachs, *Phys. Rev. A* **56**, 4755 (1997).
- [7] R. J. Brecha, L. M. Pedrotti, and D. Krause, *J. Opt. Soc. Am. B* **14**, 1921 (1997).
- [8] Y. Takubo, K. Muroo, S. Miwa, K. Yamamoto, K. Suzuki, and M. Yamamoto, *J. Mol. Spectrosc.* **178**, 31 (1996).
- [9] Y. Takubo, K. Suzuki, K. Muroo, and M. Yamamoto, *J. Mol. Spectrosc.* **184**, 78 (1997).
- [10] M. H. Anderson, J. R. Ensher, M. R. Matthews, C. E. Wieman, and E. A. Cornell, *Science* **269**, 198 (1995).
- [11] M. R. Andrews, C. G. Townsend, H.-J. Miesner, D. S. Durfee, D. M. Kurn, and W. Ketterle, *Science* **275**, 637 (1997).
- [12] J. M. Doyle, B. Friedrich, J. Kim, and D. Patterson, *Phys. Rev. A* **52**, R2515 (1995).

- [13] J. Kim, B. Friedrich, D. P. Katz, D. Patterson, J. D. Weinstein, R. DeCarvalho, and J. M. Doyle, *Phys. Rev. Lett.* **78**, 3665 (1997).
- [14] R. Engeln, G. Berden, E. van den Berg, and G. Meijer, *J. Chem. Phys.* **107**, 4458 (1997).
- [15] B. Friedrich and D. R. Herschbach, *Z. Phys. D* **24**, 25 (1992).
- [16] A. Slenczka, B. Friedrich, and D. Herschbach, *Phys. Rev. Lett.* **72**, 1806 (1994).
- [17] J. K. G. Watson, *Can. J. Phys.* **46**, 1637 (1968).
- [18] C. Amiot and J. Verges, *Can. J. Phys.* **59**, 1391 (1981).
- [19] G. Rouillé, G. Millot, R. Saint-Loup, and H. Berger, *J. Mol. Spectrosc.* **154**, 372 (1992).
- [20] M. Tinkham and M. W. P. Strandberg, *Phys. Rev.* **97**, 937 (1955); **97**, 951 (1955).
- [21] G. Herzberg, *Molecular Spectra and Molecular Structure I: Spectra of Diatomic Molecules* (Van Nostrand Reinhold, New York, 1950).
- [22] A. O'Keefe and D. A. G. Deacon, *Rev. Sci. Instrum.* **59**, 2544 (1988).
- [23] R. T. Jongma, M. H. G. Boogaarts, I. Holleman, and G. Meijer, *Rev. Sci. Instrum.* **66**, 2821 (1995).
- [24] J. H. Van Vleck, *The Theory of Electric and Magnetic Susceptibilities* (Oxford University Press, London, 1932).
- [25] R. N. Zare, *Angular Momentum* (Wiley, New York, 1988).
- [26] W. Gordy and R. L. Cook, *Microwave Molecular Spectra*, 3rd ed. (Wiley, New York, 1984).
- [27] W. H. Schaffer and J. D. Louck, *J. Mol. Spectrosc.* **3**, 123 (1959).
- [28] In Ref. [27] the denominator of the third term in Eq. (15d) should be  $4(2J-1)(2J+1)$  instead of  $4(2J+1)(2J+1)$ .
- [29] W. H. Schaffer, *J. Mol. Spectrosc.* **1**, 69 (1957).